Evolution of spin dynamics across the discontinuous metal-insulator transition in a deformable lattice

Gayan Prasad Hettiarachchi,[1,2,*] Yoshifumi Nishida,[1] Yusuke Masaki,[1]
Mohd Nazlan Mohd Muhid,[3] and Halimaton Hamdan[3]
[1]*Department of Physics, Osaka University, Toyonaka, Osaka 560-0043, Japan*
[2]*The School of Graduate Studies, Rutgers University, New Jersey 08901, USA*
[3]*Department of Chemistry, University of Technology Malaysia, 81310 Skudai, Johor, Malaysia*

(Received 10 January 2019; revised manuscript received 23 March 2019; published 24 September 2019)

We performed electron spin-resonance (ESR), magnetic, and optical absorption studies of a model system used to investigate the metal-insulator transition in a deformable lattice. The ESR and magnetic studies revealed that the small polarons have no correlation to the conductivity below or above the mobility edge. The conducting transition is marked by the appearance of an asymmetric ESR signal simultaneously with a significant suppression of the small bipolaron optical absorption band indicating that the extended states result from an abrupt dissociation of the small bipolarons. Immediately above the mobility edge competing phases of extended states, small polarons, and small bipolarons coexist. We propose a phase diagram for the charge and spin dynamics of an interacting gas of small (bi)polarons across the discontinuous conducting transition that has implications for understanding the long-standing conundrum of Mooij correlations.

DOI: 10.1103/PhysRevB.100.125154

I. INTRODUCTION

Recent studies on the metal-insulator transition (MIT) peer into the nontrivial interplay of electron correlation, electron-lattice interaction, and the random electronic potential [1–5]. If one prevails, we encounter the extreme ends of the MIT. For a disorder dominant picture, the transition is of the Anderson type [6,7]. If electron-electron interactions dominate, a Mott-Hubbard transition occurs [8–10]. In the face of non-negligible electron-lattice interactions, Mooij correlations [11] are expected to surface near the MIT or superconductor-insulator transition (SIT) [12,13] giving rise to anomalous electron transport exhibiting a negative temperature coefficient of resistivity and finite conductivity at zero temperature. When all three effects play important roles, Boltzmann and Bloch-Grüneisen transport theories fail [14], and condensed-matter physics encounters a difficult problem that is unresolved.

Theoretical and experimental studies exploring the interplay of the aforementioned effects discussed: (1) the opening of a mobility gap due to the formation of polarons [1,15,16], (2) polaron relaxation and hopping conduction with increased electron-electron interactions below the mobility edge [2,4], and (3) a (dis)continuous closing of the gap with increasing polaron *density* [2,3,17]. Recent experimental studies highlighted the intertwined effects of the electron-lattice coupling strength λ and the random electronic potential W on the conducting transition [2–4,17] using X-doped $X_{1.95-\delta}Al_{1.95}Si_{2.05}O_{8.00}$ (abbreviated as X_n/X_2-P; X = Na, K, Rb, or Cs; n is the average number of guest X atoms per formula unit) as a model system. The majority of quasiparticles in these studies were discussed terms of small bipolarons (explaining the nonmagnetic properties) coexisting with a minority of small polarons ($<3\%$ of the guest electrons) [2,3,17]. Theoretical investigations discussing the formation of small (bi)polarons in disordered systems [7,18,19] showed that a small bipolaron formed against sufficiently low on-site Coulomb repulsion energy U stabilizes at lower energy than two small polarons [15,16,20]. This suggests that the charge carriers below and possibly above the mobility edge observed in the experiments would, in theory, originate from the minority of small polarons. If this does not hold true, one would expect a tip in the energy balance between the two types of quasiparticles due to the influence of a cohort of interaction-driven parameters in a *dynamic many-polaron* system as the mobility edge is approached from the insulating side. This is yet to receive theoretical and experimental attention.

In clarifying this, we gauged the charge-carrying species and the spin dynamics of the K-doped K_2-P system (abbreviated as K_n/K_2-P) through electron spin-resonance (ESR), magnetic, and optical absorption studies. We found no correlation between the small polarons and transport properties below or above the mobility edge. Optical absorption studies indicated a continuous weakening of the binding energy of small bipolarons as the mobility edge is approached from the insulating side, followed by a partial and abrupt dissociation of these states across the mobility edge. The results suggest a tip in the energy balance between small polarons and small bipolarons well below the mobility edge giving rise to hopping conduction and, subsequently, between small bipolarons and a large polaron giving rise to extended states with increasing density in a many-polaron system. We propose a phase diagram for the three competing phases in the face of U, λ, W, and the electron transfer energy t. The subtle interplay among these parameters determines the dominant polaronic phase in

*gayan.hettiarachchi@rutgers.edu

a multiphase system, which is critical in understanding Mooij correlations near the MIT or SIT.

II. EXPERIMENTAL

Powder samples of K_n/K_2-P (dilute doping and $n = 0.09$, 0.20, 0.31, 0.39, 0.52, 0.62, 0.69, 0.81, 0.90, 1.00, and 1.09) were synthesized using a process described in the literature [17]. Details of the X_2-P structure can be found elsewhere [2,21]. The ESR spectra at room temperature (RT) of samples sealed inside glass tubes were obtained using a Bruker electron paramagnetic resonance EMX spectrometer at X-band microwave frequencies ($f = 9.6$ GHz). The temperature dependence of the ESR spectra was measured in the range of 4–300 K. The DC magnetization was measured using a superconducting quantum interference device magnetometer (Quantum Design magnetic property measurement system XL) in the temperature range of 1.8–300 K. The Curie constant C of the samples was estimated using the Curie-Weiss analysis of the temperature dependence of the magnetic susceptibility (C is 2.44×10^{-3} K emu cm^{-3} at 100% occupancy of localized spin-1/2 magnetic moments). The diffuse reflectance $r(\omega)$ was measured at RT using a UV-VIS-near-infrared spectrometer (Cary 5G, Varian) and a Fourier-transform infrared spectrometer (Nicolet MAGNA 550). The optical absorption was obtained using the Kubelka-Munk transformation $k/s = (1 - r)^2/2r$ [22], where k and s are the absorption and scattering coefficients, respectively.

III. RESULTS AND DISCUSSION

The ESR spectrum of K_{Dilute}/K_2-P (dilutely doped sample) is shown in Fig. 1. The spectrum shows a ten-line hyperfine structure with a period of 13.2 Oe and a g value of 1.9989 at the center of the ten lines. When an electron interacts with N-equivalent nuclei, the hyperfine structure shows $2NI + 1$ lines. The natural abundance ratio of the ^{39}K nucleus ($I = 3/2$) is 93.1%. Therefore, the ten-line hyperfine structure ($N = 3$) is attributed to K_3^{2+} paramagnetic small polarons where a self-trapped s electron is shared by three equivalent K cations. Note, the total spectral shape can only be reproduced with a combination of a: (1) ten-line hyperfine structure, (2) Gaussian-like signal, and (3) sharp Lorentzian signal with low intensity, which represents the magnetic impurity in K_2-P (not shown here). Hence, paramagnetic small polarons other than K_3^{2+} type are also formed at dilute doping.

The n dependence of the ESR signal at room temperature is also shown in Fig. 1 for selected samples. At $n = 0.09$, a Gaussian-like line shape is observed, which is best fit with two components $c1$ and $c2$. Component $c1$ with full width at half maximum (FWHM) of 5.8 Oe is comparable to signal (2) used to fit K_{Dilute}/K_2-P and $c2$ (FWHM $\approx$ 19 Oe) is a narrowed signal of the hyperfine structure. Similar line shapes are observed in the insulating samples up to $n = 1.00$, which are best fit with $c1$ and $c2$ components. At $n = 1.09$, an asymmetric Dysonian [23] line shape is observed. This coincides with the reported discontinuous transition to extended states probed through transport measurements [17]. The asymmetric shape is characterized by the ratio of peak heights above (A) and below (B) the baseline ($A/B \approx 2.5$). The ESR signal at

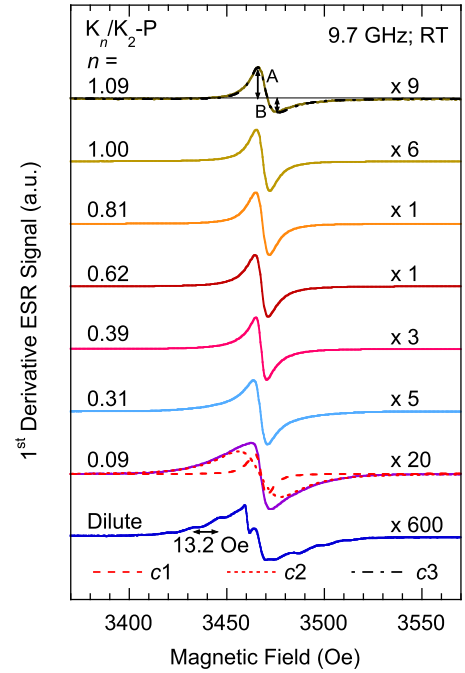

FIG. 1. The n dependence of the ESR signal at room temperature. Samples from $n = 0.09$ up to 1.00 are fit with two Lorentzian components $c1$ and $c2$. At $n = 1.09$, an asymmetric ESR signal is observed, which is fit with a Dysonian component $c3$.

$n = 1.09$ is fit with an asymmetric Dysonian line-shape $c3$. Even though the inclusion of $c1$ and $c2$ components lead to a slight increase in fitting quality, we refrain from doing so because it is insignificant.

The n dependence of the FWHM, g value, percentage of spin-1/2 magnetic moments, and electrical resistivity ρ at 300 K are shown in Figs. 2(a)–2(d), respectively. The FWHM and g value of $c1$ and $c2$ components show a drop approaching $n \approx 0.4$ (the drop in $c1$ is not clear in comparison to $c2$) coinciding with the site-percolation threshold $P_c (= 0.35)$ proposed for paired constituents in a diamond lattice [24]. Note that the cage voids of the X_2-P structure form a diamond lattice [2,21]. Afterwards, FWHM values remain invariant and the g values show a slight decrease up to $n = 1.00$ (immediately below the mobility edge). The percentage of spin-1/2 magnetic moments increases up to $n = 1.00$. The values of ρ at 300 K show a gradual decrease up to $n = 1.00$ and abruptly drop by four orders of magnitude across the mobility edge at $n = 1.09$. Above the mobility edge, FWHM shows a significant increase whereas the g value and percentage of spin-1/2 magnetic moments maintain the trend observed below the mobility edge. The increase in FWHM across the conducting transition is attributed to an enhanced spin-flip relaxation caused by the increased mobility of carriers. Note that the spin percentage does not reciprocate the change in ρ across the mobility edge indicating that the extended states are of a different origin from small polarons.

Previous reports discussed the appearance of hopping conduction and polaron relaxation at $n \gtrsim 0.69$ [4]. To confirm whether hopping is due to thermally activated carriers from ESR-active small polarons, we measured the temperature

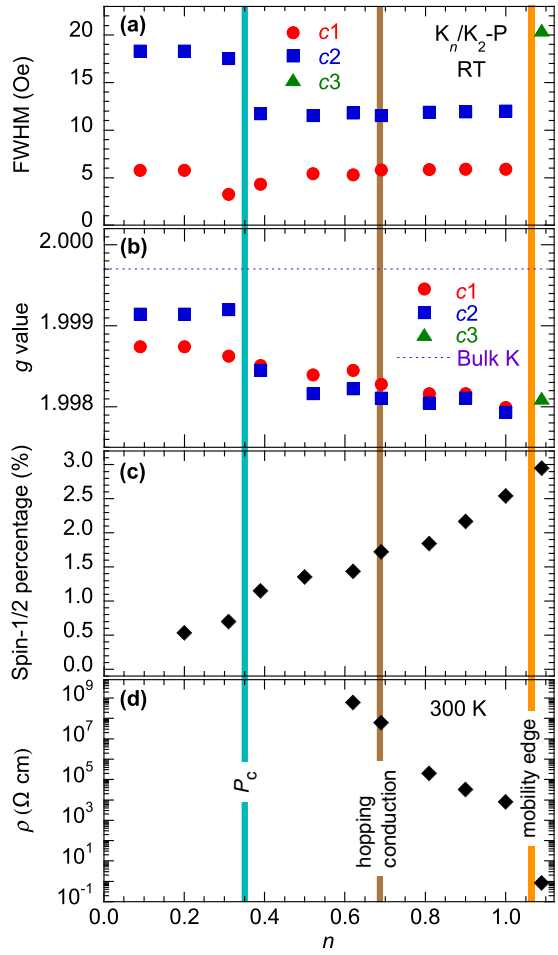

FIG. 2. The n dependence of ESR [(a) room temperature FWHM and (b) g value], magnetic [(c) percentage of spin-1/2 magnetic moments], and transport properties [(d) electrical resistivity at 300 K] of K_n/K_2-P. Note that the asymmetric $c3$ component applies only to $n = 1.09$.

dependence of the ESR signal and extracted the FWHM of the $c1$ and $c2$ components. Representative data of $n = 0.90$ is shown in Fig. 3(a). We do not see a correlation between the temperature evolution of the FWHM, which shows a variation within one order of magnitude between 10 and 300 K, and ρ [shown in Fig. 3(b)], which shows a variation of five orders of magnitude between 150 and 300 K. Note that thermally activated carriers disappear below 150 K. If the ESR signal is due to electron hopping among unpaired localized states, the inhomogeneous and hyperfine widths would be averaged by the motion whose rate can be estimated from the conductivity to be faster than the Larmor frequency at room temperature, and the line would broaden as the hopping rate drops with decreasing temperature. Such correspondence is not observed. Therefore, the ESR signal observed in the doping region exhibiting hopping conduction is not associated with temperature-activated hopping of small polarons. Above the mobility edge, if the conductivity is due to the motion of delocalized carriers, the linewidth would be due to spin-flip scattering from phonons and/or other scattering centers (localized polarons) and would decrease below the Debye

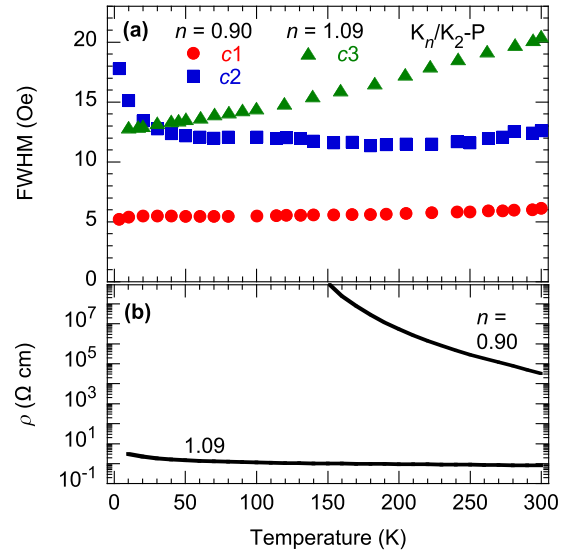

FIG. 3. The temperature dependence of (a) FWHM of the $c1$, $c2$, and $c3$ components and (b) ρ of $n = 0.90$ and 1.09. Component $c3$ applies only to $n = 1.09$.

temperature [25,26]. The FWHM ($c3$ component) at $n = 1.09$ shows a corresponding temperature dependence [Fig. 3(a)] originating from the diffusive carriers of extended states.

We used optical absorption measurements to observe the evolution of small (bi)polarons with n. The optical absorption spectra of $n = 0.09$ and other selected samples at RT are shown in Figs. 4(a) and 4(b), respectively. At $n = 0.09$, an absorption band is observed at approximately 10 600 cm^{-1} (solid circle) in agreement with previous reports [17]. Since the majority of electrons are in a paired state, this absorption is assigned to optical excitations of small bipolarons. We fit this absorption band using the small (bi)polaron absorption

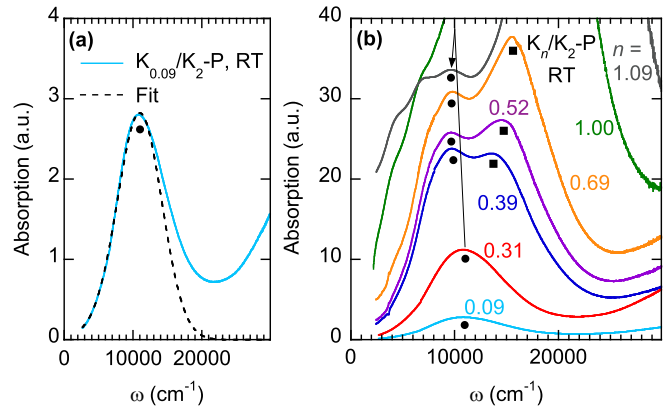

FIG. 4. The n dependence of room-temperature optical absorption spectra of K_n/K_2-P at (a) $n = 0.09$ and (b) 0.09–1.09. The solid circles and squares mark the small bipolaron and high-frequency bands, respectively. The broken curve in panel (a) is the fitting of Eq. (1). The tilted straight line and downward arrow in panel (b) provide guides for the eye to observe the evolution of the small bipolaron absorption band.

spectrum given by [27,28]

$$\alpha(\omega) = \frac{2(\pi)^{3/2}e^2}{m^*\omega c}\frac{t}{\Delta}\exp\left[-\frac{(2E_b - \hbar\omega)^2}{\Delta^2}\right], \qquad (1)$$

where m^* is the effective electronic mass, c is the speed of light, $t \equiv \hbar^2/2m^*a^2$, $\hbar$ is the reduced Planck constant, a is a lattice constant, E_b is the binding energy, $\Delta \equiv \sqrt{8E_bE_{vib}}$, and E_{vib} is the characteristic vibrational energy. The $\alpha(\omega)$ term gives the absorption coefficient per unit small-(bi)polaron *density*. A small polaron exhibits an asymmetric absorption at the resonant excitation energy $\hbar\omega = 2E_b$ [28]. For an intrasite small bipolaron, the excitation energy is $4E_b - U$ [28,29]. Since U is large (>5 eV) in this case, the small bipolarons are plausibly intersite [2,17], i.e., paired states of two small polarons at adjacent sites. Hence, we use Eq. (1) without any transformation to fit [broken curve in Fig. 4(a)] the absorption spectrum of $n = 0.09$. This gives $E_b = 0.75 \pm 0.02$ and $E_{vib} = 0.035$ eV. We are unable to isolate and assign optical absorption(s) to the minority ESR-active small polarons, which may have negligible effects on the total absorption spectrum. Therefore, we cannot approximate E_b of small polarons. According to theory [15,16], we conjecture that these have a weaker $E_b(<0.75$ eV).

The excitation energy of the small bipolaron band remains constant up to $n = 0.31$ (immediately below P_c). At $n = 0.39$, it shifts to lower frequency, and a new absorption band appears at high frequency (HF; solid square). With a further increase in $n(>0.39)$, the small bipolaron and HF bands show a redshift and blueshift, respectively. Additional midinfrared (MIR) bands appear at high n. Since our primary interest is in the small bipolaron absorption, we do not discuss HF and MIR bands for which explanations can be found elsewhere [4,17]. The redshift of the small bipolaron band starting at $n = 0.39$ [tilted straight line in Fig. 4(b)] and the abrupt suppression of its intensity at $n = 1.09$ [downward arrow in Fig. 4(b)] are, however, of significant interest in understanding the spin dynamics and subtle changes in the energy balance of the polaronic states as discussed later.

The total atomic character of the K_3^{2+}-type small polaron observed at dilute doping is evaluated to be 48% from the period 13.2 Oe compared with the four hyperfine lines separated by 82.4 Oe in isolated ^{39}K atoms. The low atomic character indicates weak confinement of the 4s electron wave function, i.e., a large t, which may favor the formation of paired states (small bipolarons) between adjacent sites even at low values of n. Hence, the minority of ESR-active small polarons are attributed to local disorder in the deformable lattice.

Around P_c, site percolation [onset of an interacting gas of small (bi)polarons] leads to changes in small polarons and bipolarons. In the case of small polarons, the ESR signal shows changes in terms of a drop in FWHM and g value. Since we do not observe any traces of conductivity below and around P_c to support motional narrowing of the ESR signal, we suggest exchange narrowing due to percolation. The g value is very low compared to bulk K, which can be attributed to spin-orbit coupling (SOC). Mixing of s and p orbitals due to deformation of the 4s electron wave function can induce SOC. Readjustments in the deformable lattice [3,4] at P_c can result in greater s-p mixing leading to a further drop in the g value. In the case of small bipolarons, optical absorption at approximately 10 600 cm^{-1} shows a redshift suggesting a weakening of E_b immediately above P_c.

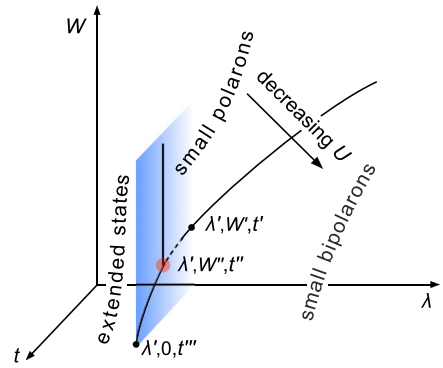

FIG. 5. The proposed phase diagram for extended states and small (bi)polarons in the face of λ, W, t, and U. See the text for details.

The small bipolaron absorption shows a continuous redshift starting at $n = 0.39$ [Fig. 4(b)] suggesting that readjustments in the deformable lattice due to site percolation and subsequent increase in n (as a result, increase in t) lead to a continuous weakening of E_b (in effect, weakening of W). In this scenario, at a critical density (in our case, $n \approx 0.6$), a tip in the energy balance between small polarons and small bipolarons occurs, and hopping conduction of small bipolarons appears due to thermal activation. The activation energy E_a is related to E_b by $E_a \approx \frac{1}{2}E_b - J$, where J is the electronic overlap integral between two adjacent sites [30]. It is noted that this relationship becomes nontrivial due to a multitude of parameters, such as W, t, and distance between hopping sites; and E_a can practically drop to zero even if E_b remains finite and high [30].

At $n = 1.09$, an abrupt suppression of the intensity of the small bipolaron absorption band [downward arrow in Fig. 4(b)] is observed simultaneously with an asymmetric ESR line shape [Fig. 1] suggesting a discontinuous tip in the energy balance between small bipolarons and a large polaron (extended states). Abrupt dissociation of small bipolarons results in the extended states. However, a weak trace of the absorption remains at $n = 1.09$ indicating that some small bipolarons coexist (due to disorder) with the extended states. Furthermore, small polarons also coexist as seen by the finite spin-1/2 magnetic moments at $n = 1.09$ [Fig. 2(c)]. Hence, $n = 1.09$ lies in a critical region where three competing phases coexist in the phase diagram of λ, W, t, and U shown in Fig. 5 (area marked in red) giving rise to anomalous electronic transport. Above P_c and below the mobility edge, on the plane of W and $t(W'' < W < W'; t' < t < t'')$ at finite and constant $\lambda(=\lambda')$, we observe a region where the energy balance between small polarons and small bipolarons continuously change (represented by a broken line). In this region, small bipolarons occupy a higher-energy level (or, at least, comparable to small polarons) giving rise to hopping conduction. At $n = 1.09$, a discontinuous change between small bipolarons and extended states occurs. We do not observe a transition between small polarons and extended states, even

though it is plausible under different conditions [15,16]. We highlight that the magnitudes of t and W together with U and λ render critical parameters affecting the balance among competing polaronic phases. We conjecture that the coexistence of competing phases and the correlated response of the lattice to the random electronic potential give rise to Mooij correlations [11] and anomalous electron-transport properties near the mobility edge [1,12,13].

To summarize, we investigated the doping evolution of spin dynamics of a model system demonstrating a discontinuous metal- (extended states-) insulator transition in a deformable lattice by performing ESR, magnetic, and optical absorption studies. Small polarons show no correlation to the conductivity below or above the mobility edge. Above the site-percolation threshold, the binding energy of small bipolarons shows a continuous weakening. Starting at a critical doping density, continuous change in the energy balance between the minority small polarons and majority small bipolarons gives rise to thermally activated carriers of small bipolarons. With a further increase in doping, partial and abrupt dissociation of small bipolarons results in a discontinuous transition to extended states. Immediately above the transition, extended states and small (bi)polarons coexist. We propose a phase diagram for the spin and charge dynamics of an interacting gas of small (bi)polarons across the discontinuous conducting transition. Studies are underway to gauge the evolution of spin dynamics near the mobility edge with subtle changes in λ.

ACKNOWLEDGMENTS

G.P.H. thanks S. Tamiya, T. Nakano, and Y. Nozue for providing experimental facilities and support. G.P.H. acknowledges financial support from the Research Promotion Division of Osaka University and the Ministry of Education, Culture, Sports, Science and Technology of Japan under the program for promoting research activities.

[1] D. Di Sante, S. Fratini, V. Dobrosavljević, and S. Ciuchi, Phys. Rev. Lett. **118**, 036602 (2017).
[2] G. P. Hettiarachchi, F. Moriasa, Y. Nishida, T. Nakano, M. N. M. Muhid, and H. Hamdan, Phys. Rev. B **96**, 155115 (2017).
[3] G. P. Hettiarachchi, M. N. M. Muhid, and H. Hamdan, Phys. Rev. B **97**, 155142 (2018).
[4] G. P. Hettiarachchi, Y. Nishida, and Y. Masaki, Phys. Rev. B **98**, 035125 (2018).
[5] S. Ciuchi, D. Di Sante, V. Dobrosavljević, and S. Fratini, npj Quantum Materials **3**, 44 (2018).
[6] P. W. Anderson, Phys. Rev. **109**, 1492 (1958).
[7] E. Abrahams, P. W. Anderson, D. C. Licciardello, and T. V. Ramakrishnan, Phys. Rev. Lett. **42**, 673 (1979).
[8] N. F. Mott, Rev. Mod. Phys. **40**, 677 (1968).
[9] N. F. Mott, Proc. R. Soc. London, Ser. A **197**, 269 (1949).
[10] J. Hubbard, Proc. R. Soc. London, Ser. A **276**, 238 (1963).
[11] J. H. Mooij, Phys. Status Solidi A **17**, 521 (1973).
[12] M. S. Osofsky, R. J. Soulen, J. H. Claassen, G. Trotter, H. Kim, and J. S. Horwitz, Phys. Rev. Lett. **87**, 197004 (2001).
[13] N. P. Breznay, M. Tendulkar, L. Zhang, S.-C. Lee, and A. Kapitulnik, Phys. Rev. B **96**, 134522 (2017).
[14] M. S. Osofsky, C. M. Krowne, K. M. Charipar, K. Bussmann, C. N. Chervin, I. R. Pala, and D. R. Rolison, Sci. Rep. **6**, 21836 (2016).
[15] M. H. Cohen, E. N. Economou, and C. M. Soukoulis, Phys. Rev. B **29**, 4496 (1984).
[16] M. H. Cohen, E. N. Economou, and C. M. Soukoulis, Phys. Rev. B **29**, 4500 (1984).
[17] G. P. Hettiarachchi, T. Nakano, Y. Masaki, M. N. M. Muhid, H. Hamdan, and Y. Nozue, J. Phys. Soc. Jpn. **84**, 014702 (2015).
[18] D. Emin and T. Holstein, Phys. Rev. Lett. **36**, 323 (1976).
[19] W. L. McMillan, Phys. Rev. B **24**, 2739 (1981).
[20] M. Kaviani, J. Strand, V. V. Afanas'ev, and A. L. Shluger, Phys. Rev. B **94**, 020103(R) (2016).
[21] B. R. Albert, A. K. Cheetham, J. A. Stuart, and C. J. Adams, Microporous Mesoporous Mater. **21**, 133 (1998).
[22] P. Kubelka and F. Munk, Z. Tech. Phys. **12**, 593 (1931).
[23] F. J. Dyson, Phys. Rev. **98**, 349 (1955).
[24] H. Holloway, Phys. Rev. B **37**, 874 (1988).
[25] R. J. Elliott, Phys. Rev. **96**, 266 (1954).
[26] Y. Yafet, Solid State Phys. **14**, 1 (1963).
[27] H. G. Reik and D. Heese, J. Phys. Chem. Solids **28**, 581 (1967).
[28] D. Emin, Phys. Rev. B **48**, 13691 (1993).
[29] A. V. Puchkov, T. Timusk, M. A. Karlow, S. L. Cooper, P. D. Han, and D. A. Payne, Phys. Rev. B **52**, 9855(R) (1995).
[30] I. G. Austin and N. F. Mott, Adv. Phys. **18**, 41 (1969).